Applied Thermal Engineering 197 (2021) 117385

Contents lists available at ScienceDirect

Applied Thermal Engineering

journal homepage: www.elsevier.com/locate/apthermeng

Experimental study of flat-disk loop heat pipe with R1233zd(E) for cooling terrestrial electronics

Runze Zhao, Zikang Zhang, Shuaicheng Zhao, Haichuan Cui, Zhichun Liu, Wei Liu *

School of Energy and Power Engineering, Huazhong University of Science and Technology, Wuhan 430074, China

ARTICLE INFO

Keywords:
Loop heat pipe
Flat-disk evaporator
Eco-friendly working fluid
Thermal performance
Terrestrial application

ABSTRACT

Flat evaporator loop heat pipes with good thermal performance and compact volume have been widely used in electronic device applications. A flat-disk evaporator loop heat pipe made of aluminum alloy was designed for terrestrial application in this paper. R1233zd(E) was selected as the working fluid for its ultra-low toxicity and environmentally friendly. The pumping force of the system, driving the working fluid circulation, was generated by the sintered capillary wick made from nickel powder. Considering the requirements for electronics and the capillary limit of the wick together, the target temperature was below 75 °C and the effective heat transfer length was set as 790 mm. With a heat sink temperature of −10 °C, it could dissipate the heat of 190 W (11.43 W/cm^2). The performance investigation under bad external conditions was also carried out. A relatively broad operating range between the heat load of 10 W (0.60 W/cm^2) and 130 W (7.82 W/cm^2) was observed with a 30 °C heat sink temperature. However, slight temperature overshoot occurred during the start-up test but the system was able to self-regulate and stabilize quickly. Moreover, the variable heat load test, imitating the heat-dissipating demand for actual electronic devices, demonstrated that this system responded fast and operation failure did not happen. The minimum thermal resistance of the evaporator and the total LHP was 0.134 °C/W and 0.197 °C/W, respectively.

1. Introduction

Loop heat pipe (LHP), having been widely used in applications after years of development, is an efficient passive heat dissipation device based on its phase change heat dissipation mechanism [1,2]. In recent years, the demand for data processing and information transfer has greatly increased, rising the energy consumption of terrestrial electronic devices, such as telecommunication equipment, computing servers, etc., finally leading to a sharp growth in heat dissipation requirements [3]. Many researchers applied LHP as thermal management equipment for terrestrial electronic devices [4–6] owing to its merits of high efficiency, robust stability, low thermal resistance, and flexible arrangement.

There are usually two shapes of evaporators, cylinder, and flat plate [2], each of which has its advantages. The flat plate evaporator contacting the heating area without a saddle contains the advantages of simpler installation, lower thermal resistance, and smaller size [7]. The cylindrical evaporator LHP has a stronger heat transfer capacity, however, the installation of a saddle leads to uneven temperature distribution and larger volume. Hence, researchers have carried out extensive researches on the flat plate evaporator LHP, especially for terrestrial applications, including the improvement of capillary wick performance, the influence of gravity, and condensation temperature, etc. Solomon et al. [8] fabricated a bio-wick made of wood material more simply and cheaply and investigated its performance in an LHP system. The experiment showed that the bio-wick performed a good ability to pump the working fluid. During the start-up tests, it could start normally in the range of 50 W to 250 W. Liu et al. [9] used chemical methods to plate copper on the surface of the carbon capillary wick. The treated carbon wick with stronger hydrophilicity obtained a better performance and was able to provide 3.11 kPa capillary pressure. Zhang et al. [10] tested the limiting performance of biporous capillary wick sintered from nickel and sodium carbonate powders. The maximum heat load could reach 330 W (heat flux of 19.9 W/cm^2) with a 3070 mm heat transfer distance at a tilt angle of 4.6°. Phan et al. [11] successfully fabricated a polydimethylsiloxane wick in an easier method. The performance of the wick was good with a maximum heat flux of 4.5 W/cm^2. A composite wick made by Xu et al. [12] could reach a maximum heat load of 140 W with a thermal resistance of 0.143 °C/W.

In addition to the studies of capillary wicks, the operating mechanism of LHP has also been broadly investigated. Chernysheva et al. [13] studied a copper–water loop heat pipe under different external

* Corresponding author.
E-mail address: w_liu@hust.edu.cn (W. Liu).

https://doi.org/10.1016/j.applthermaleng.2021.117385
Received 16 April 2021; Received in revised form 23 June 2021; Accepted 21 July 2021
Available online 26 July 2021

Nomenclature

Q	heat load, W
R	thermal resistance, °C/W
T	temperature, °C
V	volume, m^3

Greek symbols

β	the fraction of vapor in the compensation chamber
ε	the porosity of the capillary wick
γ	the fraction of vapor in the condenser

Subscripts

c	condenser
cc	compensation chamber
evap	evaporator
h	heating area
ll	liquid line
total	total LHP

Abbreviations

Amb	ambient
Comp-wall	the wall of the compensation chamber
Cond-inlet	the inlet of the condenser
Cond-outlet	the outlet of the condenser
Evap-inlet	the inlet of the evaporator
Evap-outlet	the outlet of the evaporator
HS	heating module surface
SS	stainless steel

conditions. The LHP operated in constant heat conduction mode at 60 °C condensing temperature without the affection of the slope. Odagiri et al. [14] carried out an experiment with the flat rectangular evaporator LHP under high heat flux at six different orientations indicating that not only the LHP orientation but also the liquid–vapor phase distribution would affect the LHP performance. Anand et al. [15] presented a miniature loop heat pipe and carried out a visual experiment with four working fluids. The experiments indicated that bubbles would appear during the performance degradation because of the intense nucleation inside the compensation chamber. The influence of non-condensable investigated by Wang et al. [16] implied the non-condensable gas deteriorated the LHP heat performance regardless of the relative position of the evaporator and condenser. Li et al. [17] designed an LHP with two forced air cooling condensers. Compared with the single condenser LHP, it appeared uneven distribution of working fluid causing condensation efficiency to be reduced.

Besides, some investigations with the purpose of practical applications were carried out with prototypes designed and tested. A squared evaporator LHP aiming at a large heating area designed by He et al. [18] was tested. The area of the rectangular flat evaporator was 54.76 cm^2. The maximum heat load could reach 160 W with the heating block temperature below 80 °C and the evaporator performed good temperature uniformity. In order to recycle waste heat of industrial equipment, Aono et al. [19] presented an LHP with the ability to transfer kW-class heat with the maximum heat load of 6.2 kW. Xiao et al. [20] tested a squared LHP for multi-heat sources. It could operate between 25 W and 140 W with the temperature of the heating surface below 90 °C. Ueno et al. [21] reduced the thickness of the evaporator to 1 mm by moving the compensation chamber to the side, using ethanol as the working fluid, and when the target temperature was within 83 °C, the heat load was 18 W. Also, some researchers reduced the thick of the LHP to millimeter level or sub-millimeter level for application in smartphones by removing the compensation chamber [22,23].

Table 1 shows the geometric parameters and thermal performance of some published LHPs for terrestrial applications. A large number of experimental studies have shown that flat evaporator LHPs have good thermal performance, but there are still several problems hindering large-scale applications on the ground. The main problem is that the standard boiling points of working fluids such as water, acetone, and methanol are relatively high, so controlling the temperature of the heating area at a low level is difficult. However, the tolerable temperature for most electronic devices is 85 °C [3] and the long-term stable operation temperature is best below 75 °C. Apart from that, the LHP needs to be flexibly arranged according to the layout of the electronic components, the effective heat transfer length of about 350 mm could satisfy small devices like laptops, desktop computers and LED. However, it might be not long enough when encountering relatively large and complicated chassis.

In this study, a flat-disk LHP was fabricated by aluminum alloy and R1233zd(E) was selected as the working fluid to reach the requirements of terrestrial applications such as good thermal performance, environmentally friendly, lighter weight, cheaper price. The length of the vapor line reflecting the distance of heat transfer was designed as 790 mm to satisfy the practical demand, mainly referring to small and medium-sized servers. In addition, a set of experimental tests of this eco-friendly LHP were launched including start-up and variable heat load tests under four different heat sink temperatures. Temperature fluctuation was observed with a low heat load resulted from intermittent replenishment of the compensation chamber. With the increase in heat load or heat sink temperature, the unstable phenomenon disappeared and the LHP responded quickly and operated stably. Moreover, the uniformly variable heat load process experienced two working modes, which were caused by the change in the quantity of heat leakage and supercooling. The main aim of this paper was to design a safe, eco-friendly, reliable, and stable LHP with good thermal performance and provide a reference for large-scale terrestrial applications.

Table 1
Summary of recent LHP investigation.

Evaporator shape/material	Working fluid	Vapor line length	Maximum heat load	Heating area	Maximum temperature	Ref.
Disk/brass	Water	140 mm	120 W	7.07 cm^2	85 °C	[24]
Disk/brass	Methanol	300 mm	160 W	9.52 cm^2	85 °C	[25]
Disk/copper	Methanol	330 mm	160 W	9.63 cm^2	90 °C	[26]
Disk/copper	Water	140 mm	140 W	7.07 cm^2	90 °C	[12]
Rectangle/SS	Acetone	110 mm	280 W	14.29 cm^2	100 °C	[14]
Rectangle/copper	Water/methanol/ethanol	330 mm	900 W/380 W/320 W	27.29 cm^2	95 °C	[27]
Rectangle/copper	Water-cooper nanofluid	350 mm	100 W	12 cm^2	66.1 °C	[28]
Rectangle/copper	Water	215 mm	75 W	6.25 cm^2	110 °C	[9]
Rectangle/copper	Water	320 mm	150 W	6.25 cm^2	85 °C	[29]

2. Design of the experiment

2.1. Working fluid selection

The working fluid of the LHP system, having a great impact on heat transfer characteristics [30], is an important factor that needs to be considered in the design. In addition to the thermodynamic properties, toxicity and flammability should also be considered for ground applications. Ammonia, thanks to the outstanding thermodynamic properties mainly referring to the large value of dP/dT, has been extensively adopted in LHP for space. The ammonia LHP has the characteristics of a small starting threshold, rapid thermal response, and low operating temperature. However, owing to high saturation pressure (2.0 Mpa at 50 °C) and strong toxicity to humans it would probably be limited in terrestrial applications. Although the thermodynamic properties of traditional organic working fluids like acetone and methanol are good, the highly toxic and flammable might cause them to be applied on specific occasions. Deionized water is safe, non-toxic, and easy to obtain, but with a high standard boiling point making the target surface hotter. The increase in the temperature of the target surface makes it suitable for use in some electronic devices with strong temperature tolerance. On the whole, terrestrial applications demand some special requirements like safety and non-toxic yet traditional working fluids might not cater to these very well. The seep of the working fluid from the LHP system cannot be completely avoided, so the issue needs to be solved at the source.

In this situation, R1233zd(E) was found and used as the working fluid. R1233zd(E), as a fourth-generation eco-friendly refrigerant, has ultra-low toxicity (non-toxic to humans), non-flammable characteristics, and good thermodynamic properties among refrigerants [31,32]. Compared with traditional working fluids, although the latent heat of R1233zd(E) is relatively small, it is a kind of isentropic fluid that will not cause liquid drops in the vapor line. Plus its environmentally friendly characteristics, it is still a preferable selection for terrestrial applications, Table 2 shows its physical properties.

2.2. LHP structural design

The mechanical structure of the loop heat pipe is composed of an evaporator, a vapor line, a liquid line, and a condenser, of which the evaporator is the most important component. A biporous wick as shown in Fig. 1 was used to provide sufficient capillary force. It had evenly distributed large and small pores, as depicted in Fig. 2. Small pores could provide large capillary force and large pores could provide channels for working fluid flow. As nickel powder has good sinterability and moderate thermal conductivity, it has been chosen as a material to make wicks. The sintering process could be divided into four steps mainly: powder processing, molding, sintering, cleaning. After being cleaned, based on the Archimedes principle, the wick porosity could be calculated as follows:

$$\varepsilon = \frac{m_1 - m_2 - m_3}{m_1 - m_4} \tag{1}$$

Table 2
The main physical properties of R1233zd(E).

Chemical formula	CF3CH = CHCl
Standard boiling point	18.26 °C
Triple point temperature	−78 °C
Critical pressure	3.6 MPa
Critical temperature	166.45 °C
Critical density	480.23 kg/m^3
Surface tension (50 °C)	0.0114 N/m
Saturation pressure (50 °C)	0.29 MPa
Latent heat of vaporization (50 °C)	177.32 KJ/kg
Saturated liquid density (50 °C)	1199.72 kg/m^3
Saturated vapor density (50 °C)	15.68 kg/m^3
ODP	0
GWP	7

Fig. 1. The main parameters of the wick.

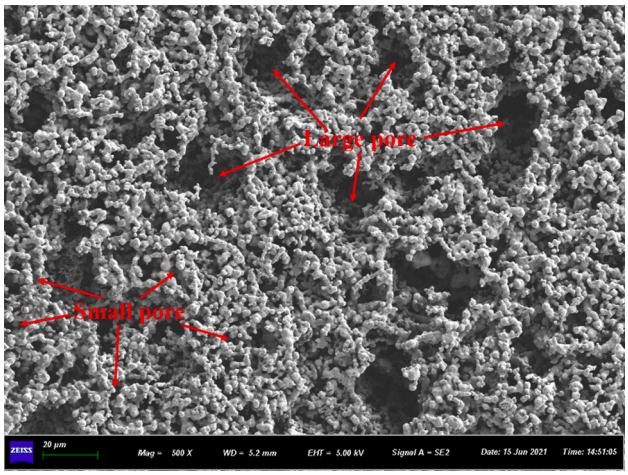

Fig. 2. Microstructure of the biporous wick at × 500 magnification.

where m_1, m_2, m_3, and m_4 denote the quality of fully wet capillary wick, fully dry capillary wick, balance bar and counterweight, the capillary wick when it is immersed in water. The porosity of the capillary wick was estimated to be 78.65% using this method.

Although the flat evaporator has advantages in thermal resistance and volume, the ability in resisting high pressure is weak. The saturation pressure of a working fluid during the operation greatly affecting the system safely, therefore, should be taken into consideration. The evaporator made of aluminum alloy, with working fluid compatibility, strength, weight, and cost into consideration, is shown in Fig. 3 (a). The saturation pressure of R1233zd(E) at 50 °C is only 0.29 Mpa, thus a relatively small value (1.5 mm) was designed as evaporator wall thickness with adequate strength and lightweight (16.9 g). And its contribution to reducing thermal resistance was proved in experiments. Static analysis was studied by Ansys 15.0, proving the safety and reliability of the evaporator could be maintained even when the internal pressure was up to 0.5 Mpa. In addition, the sealing between the capillary wick and evaporator shell has a great influence on the performance of the loop heat pipe. If there is no good encapsulation between them, the system performance will deteriorate, such as startup failure owing to the vapor side leakage and evaporator thermal resistance increase owing to the inadequate contact. In the first step, the direction of the wick should be adjusted so that the vapor channels would be parallel to the vapor outlet, and then the wick was slowly pressed into the stepped hole inside the evaporator shell forming a slightly tight transition fit between them, as shown in Fig. 3 (a). After that, the cover plate would be pressed into the shell and it was necessary to press it using a clamp to ensure that the wick could contact the cover plate adequately. In the last stage, low-temperature aluminum welding was applied to weld the cover plate and the shell, and argon gas was passed into the evaporator to protect the capillary wick during the whole process.

In order to reduce the flow resistance of the working fluid, the inner diameters of the vapor line and the liquid line were set as 8 mm and 6

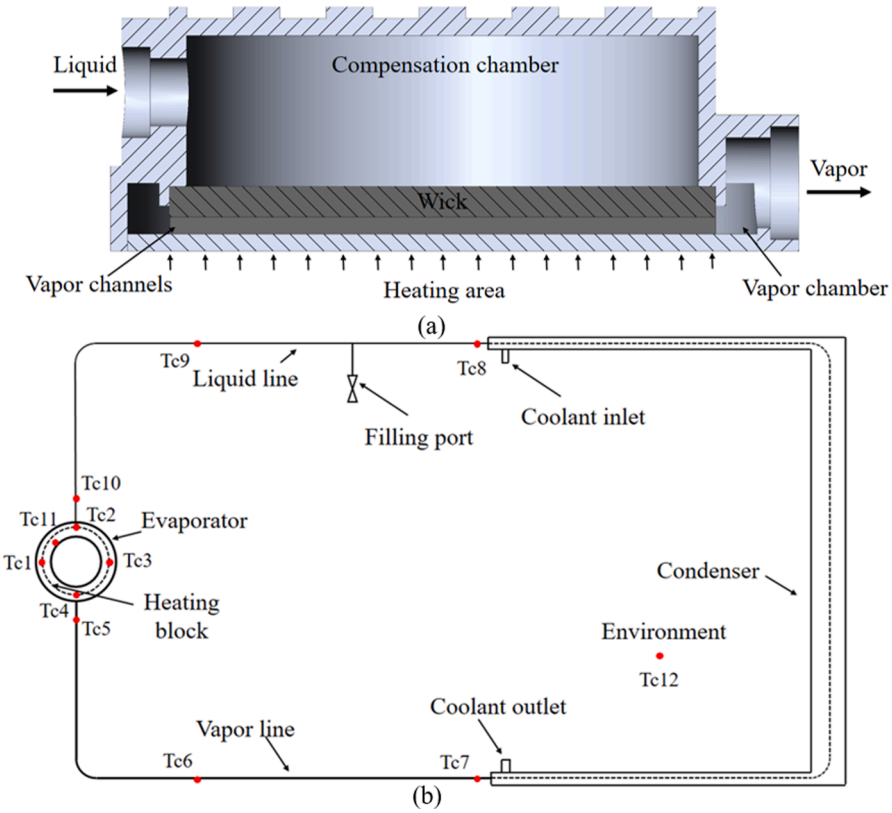

Fig. 3. (a) The structure of the evaporator. (b) The diagram of the LHP and the arrangement of the thermocouples.

mm, respectively. The pipe-in-pipe condenser connecting with a chiller was adopted to condense the vapor into subcooled liquid. Fig. 4 depicts the configuration and dimension of the LHP prototype all made of aluminum alloy 7075. Table 3 gives the main parameters of each part.

2.3. Test method

A copper block with 4 cartridge heaters was designed as the heating module having a heating area of 16.62 cm^2. During the experiment, the heating power was changed by a voltage regulator and measured by a power meter with 0.5% accuracy. As depicted in Fig. 3 (b), 12 T-type thermocouples with an accuracy of ± 0.3 °C were arranged to monitor the temperature of each key part of the LHP. The temperature of the heating area was measured by Tc1, Tc2, Tc3, and Tc4. Along the direction of the working fluid flow, Tc5, Tc6, and Tc7 were arranged at the starting point, the midpoint, and the endpoint of the vapor line. The arrangement of Tc8, Tc9, and Tc10 on the liquid line was similar to that of the vapor line. Tc11 and Tc12 were used to monitor the temperature

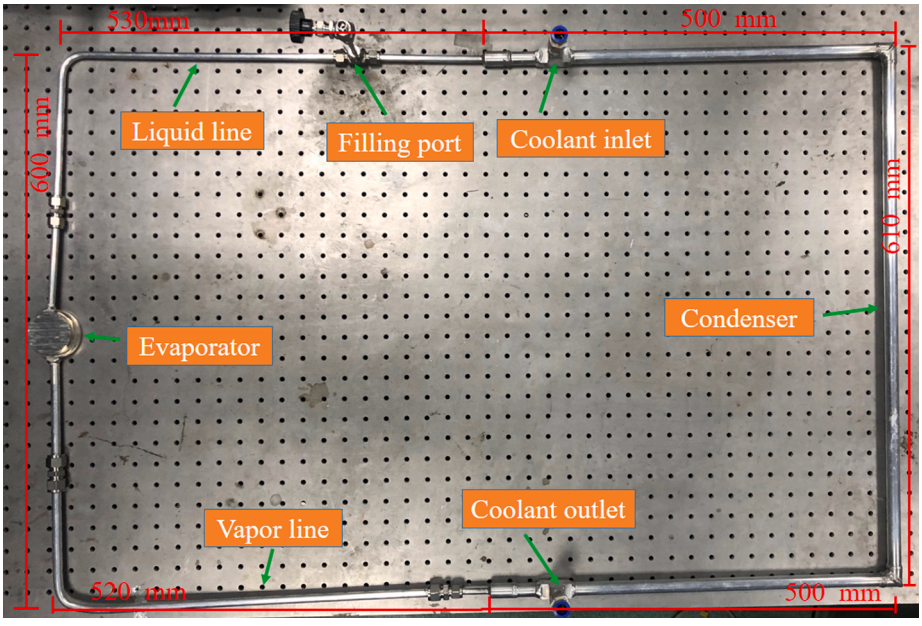

Fig. 4. Configuration and dimension of the LHP prototype.

Table 3
The main parameters of the LHP.

Evaporator	Overall height	21.8 mm
	Diameter	58.6 mm
	Heating area	16.62 cm^2
Wick	Diameter	47.73 mm
	Height	3.97 mm
	Number of grooves	13
	Width/height of the groove	2/1.5 mm
	Large/small pore diameter	20.21/2.58 μm
	Thermal conductivity	2.55 W/m·K
	permeability	3.9×10^{-13} m^2
	Porosity	78.65%
	Material	Nickel
Vapor line	Inner/outer diameter	8/10 mm
	Length	790 mm
Liquid line	Inner/outer diameter	6/8 mm
	Length	800 mm
Condenser	Inner/outer diameter of inner pipe	14/16 mm
	Inner/outer diameter of outer pipe	6/8 mm
	Length	1610 mm

of the compensation chamber and the environment respectively. The data collector "Keithley 2700" was used to collect and record temperature signals every 3 s. A chiller with an accuracy of ± 0.1 °C was connected with the condenser to cool down the working fluid. Both the heating module and the LHP were wrapped with insulation materials (NBR/PVC, thermal conductivity 0.04 W/m·K) to reduce the impact of environmental heat leakage. According to the vapor–liquid distribution during the normal operation of the LHP, the charging ratio was calculated to be 59.74%. Non-condensable gas would cause deterioration of the LHP performance, so the system was evacuated by a molecular pump unit before charged with R1233zd(E). The loop heat pipe was evacuated to 10 Pa by a mechanical pump and then to 3.2×10^{-4} Pa by a molecular pump. Experiments were carried out at four heat sink temperatures of −10 °C, 0 °C, 15 °C, and 30 °C, respectively. The position of the condenser was 1 cm higher than that of the evaporator during the experiments.

3. Results and discussion

3.1. Start-up performance tests

Start-up performance is an important character of LHP. With heating area temperature below 75 °C, the LHP could start successfully within the heat load range of 10 W to 190 W. As described in Fig. 5 (a) and Fig. 5 (b), there were similar start-up processes when the sink temperature was −10 °C and 0 °C respectively. Due to the good thermal conductivity of aluminum alloy, at the beginning of the start, the temperature of each measuring point was lower than the ambient temperature and the condenser was the coldest part. Additionally, the condenser was fulfilled with liquid, but other parts were in a vapor–liquid mixed state according to the charging ratio. When the heat load was applied, the temperature of the condenser inlet rose evenly and slowly, indicating a small number of vaporization cores in the evaporator made the working fluid continuously vaporize. However, such a small vapor driving force could not overcome the gravity resistance of the two-phase flow in the vapor line. Only when the vapor was cumulated to a certain amount, could the accumulated two-phase mixture be pushed back to the compensation chamber, which assisted the vapor–liquid distribution in returning to the normal condition. After that, the resistance of the working fluid flow dropped and the vapor in the

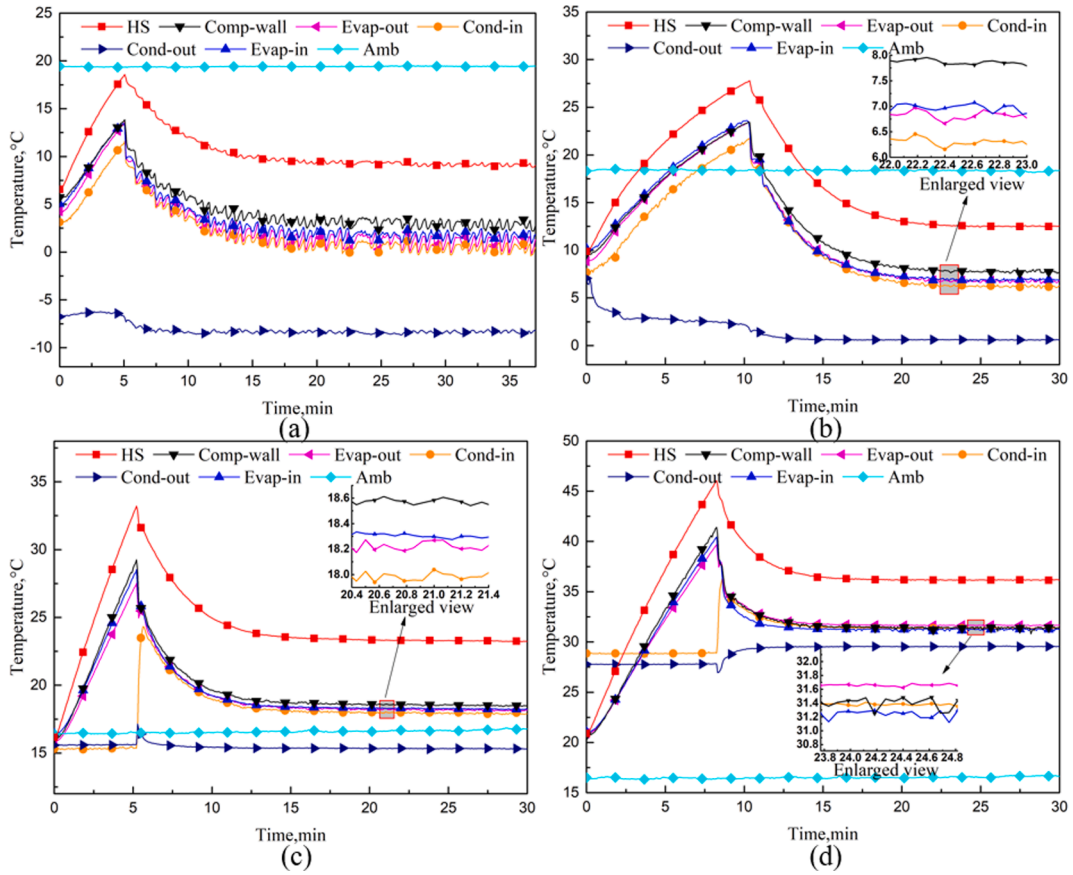

Fig. 5. The thermal performance in start-up process of 30 W with different heat sink temperatures. (a) T_{sink} = -10 °C. (b) T_{sink} = 0 °C. (c) T_{sink} = 15 °C. (d) T_{sink} = 30 °C.

compensation chamber was eliminated gradually by subcooled liquid. Under the automatic adjustment of the capillary wick, the vapor pressure and the evaporator temperature decreased, then the temperature of each part gradually stabilized. It is seen in Fig. 5 (c) and Fig. 5 (d) that temperature overshot was also observed. Compared with Fig. 5 (a) and Fig. 5 (b), the evaporator was fulfilled with liquid at the beginning of the start in these conditions deducing from the filling ratio so that there were no vaporization cores in it at the moment. After the heat load was applied for several minutes, the superheated liquid vaporized in a sudden pushing the subcooled liquid back to the compensation chamber, then the temperature of each measuring point plummeted, and finally stabilized under the joint function of the heating module, condenser, and environment.

As shown in Fig. 5 (a), the temperature of the condenser inlet fluctuated in a small zigzag shape, which was caused by the joint function of gravity and the mismatch between the evaporation rate and the condensation rate. When the vapor entered the condenser, the vapor pressure decreased dramatically which was not enough to push the subcooled liquid to go back to the compensation chamber. At this time, due to the dearth of liquid in the compensation chamber, the capillary wick was insufficiently supplied with liquid and gradually got dry so the operation temperature increased. Before the capillary wick was completely dried, the accumulated vapor overcame the gravity head so the liquid was pushed to the compensation chamber. As a result, the gravity became the driving force from resistance and the capillary wick got adequate supplement. Therefore, the operation temperature decreased. However, this process did not last for long for the reason that the condensation was too strong that vapor pressure dropped again and the LHP returned to the status waiting for vapor accumulation.

Besides, another phenomenon was observed in Fig. 5: the lower the heat sink temperature, the larger the temperature fluctuation range. When the LHP is operating normally, the density of the liquid is much greater than the vapor's, so the liquid volume can be calculated by Eq. (2),

$$V_{charge} = V_{ll} + \varepsilon V_{wick} + (1-\beta)V_{cc} + (1-\gamma)V_c \tag{2}$$

where V_{charge}, V_{ll}, V_{wick}, V_{cc}, V_c, are the volume of the filled liquid, the liquid line, the wick, the compensation chamber, and the condenser, respectively; ε denotes the porosity of the wick, β denotes the fraction of vapor in the compensation chamber, and γ denotes the fraction of vapor in the condenser. With the condensing temperature decreasing, γ will decrease due to the stronger condensing capacity. However, V_{charge} is a constant value, so β needs to increase to satisfy the Eq. (2). This indicates the lower the condensation temperature, the more the vapor volume in the compensation chamber. The compensation chamber with less liquid is more susceptible to the fluctuation of the vapor–liquid interface in the condenser. Moreover, less liquid cannot effectively prevent the growth and annihilation of vapor accompanying by temperature fluctuations. Hence temperature fluctuation was more drastic when the heat sink temperature was −10 °C and gradually weakened with the increase in the heat sink temperature.

When the temperature of the heat sink was not changed, the modes of the start-up process could be classified into four patterns with the increase in the heat load, namely failure mode, fluctuation mode, overshot mode, and normal mode according to Ref. [33]. Before the loop heat pipe operated, the liquid in the compensation chamber was easy to vaporize since the sidewall heat leakage and back heat leakage. As a result, the loop heat pipe could not start up successfully when the heat load applied was under a certain value called starting threshold and this mode was called failure mode. The experimental tests showed that this loop heat pipe could finish the start-up process successfully with a heat load of 10 W, as shown in Fig. 6 (a). As depicted in Fig. 6 (b), when the heat load increased to 50 W, obvious temperature oscillation and overshot were observed simultaneously since these detrimental phenomena were caused by the small vapor generation rate. The lower rate of the vapor generation could not push the liquid back to the compensation chamber in the beginning until the amount of superheated vapor accumulated enough. The temperature overshot, therefore, was observed. Meanwhile, the subcooled liquid could only return to the compensation chamber intermittently due to the small generation rate of the vapor. As a result, the zigzag temperature fluctuation was observed. When the heat load grew to 110 W, the vapor generation rate was large enough so the temperature overshot and fluctuation nearly disappeared as described in Fig. 6 (c) and the loop heat pipe entered into normal start-up mode. As shown in Fig. 6 (d), once a large heat load was applied, the liquid in the vapor chamber and vapor channel obtained a large degree of superheat instantly, establishing the temperature difference and the pressure difference between them and the compensation chamber. Under the pressure difference, the working fluid flowed into the condenser and then backed to the compensation chamber. When the temperature of the compensation chamber reached equilibrium, the capillary force formed by the vapor–liquid meniscus did not change anymore. Also, the sum of capillary force and vapor driving force was exactly equal to the pressure drop of the circulation. The LHP finished its start-up process and entered a steady state.

3.2. Performance tests with variable heat load

The reliability of LHP with variable heat load is another important character. Fig. 7 and Fig. 8 depict the thermal performance of the LHP at heat sink temperature of 15 °C with uniformly and randomly variable heat load respectively. With the temperature of the heating area below 75 °C, the heat load varied from 30 W to 150 W and finally backed to 30 W. Fig. 7 presents that the LHP responded quickly when the heat load changed and the temperature fluctuation had not appeared with the heat sink temperature of 15 °C. Although under the same external conditions, owing to the former vapor–liquid distribution and thermal state, the performance of the LHP during the decrease stage of the heat load was worse than that during the increase stage. When the heat load was 130 W, the temperature of the heated area in descending stage was 2 °C higher than that in the rising stage. When the heat load was 110 W and 90 W, the values were 1 °C and 0.8 °C, respectively. The pressure of the vapor and the liquid decreased as the heat load went down, making the saturated liquid superheated and unstable. However, the heat leakage from the heating area to the compensation chamber did not correspondingly reduce. Therefore, the superheated liquid was easier to vaporized, increasing the fraction of the vapor of the compensation chamber with the heat transfer ability deteriorating, and finally, resulting in the temperature hysteresis.

As illustrated in Fig. 8, no matter how the heat load changed, the LHP could adjust to a stable state in about 10 min. With a growth in the heat load, the amount of working fluid vaporization and flowing resistance went up, making the vapor–liquid meniscus of the wick regulate to obtain higher vapor pressure and temperature in the evaporator. On the contrary, a counter regulative process appeared as the heat load declined. Above all, the aluminum alloy-R1233zd(E) LHP responded fast within a large heat load range, reaching the practice application requirements.

3.3. The characteristic temperature analysis

Fig. 9 depicts the relationship between characteristic temperature and heat load with different heat sink temperatures. The maximum heat load still reached 130 W (7.82 W/cm^2) when the temperature of the heat sink was 30 °C. As the heat sink temperature went down, the amount of subcooling of the liquid increased. Thus, for the same heat load condition, the evaporator inlet attained a lower temperate, leading to a decline in the temperature of the compensation chamber and the heating area, so that the corresponding maximum heat load would go up. Owing to the experimental results, the maximum heat load was 190 W (11.43 W/cm^2), 170 W (10.23 W/cm^2), and 150 W (9.03 W/cm^2) with the heat

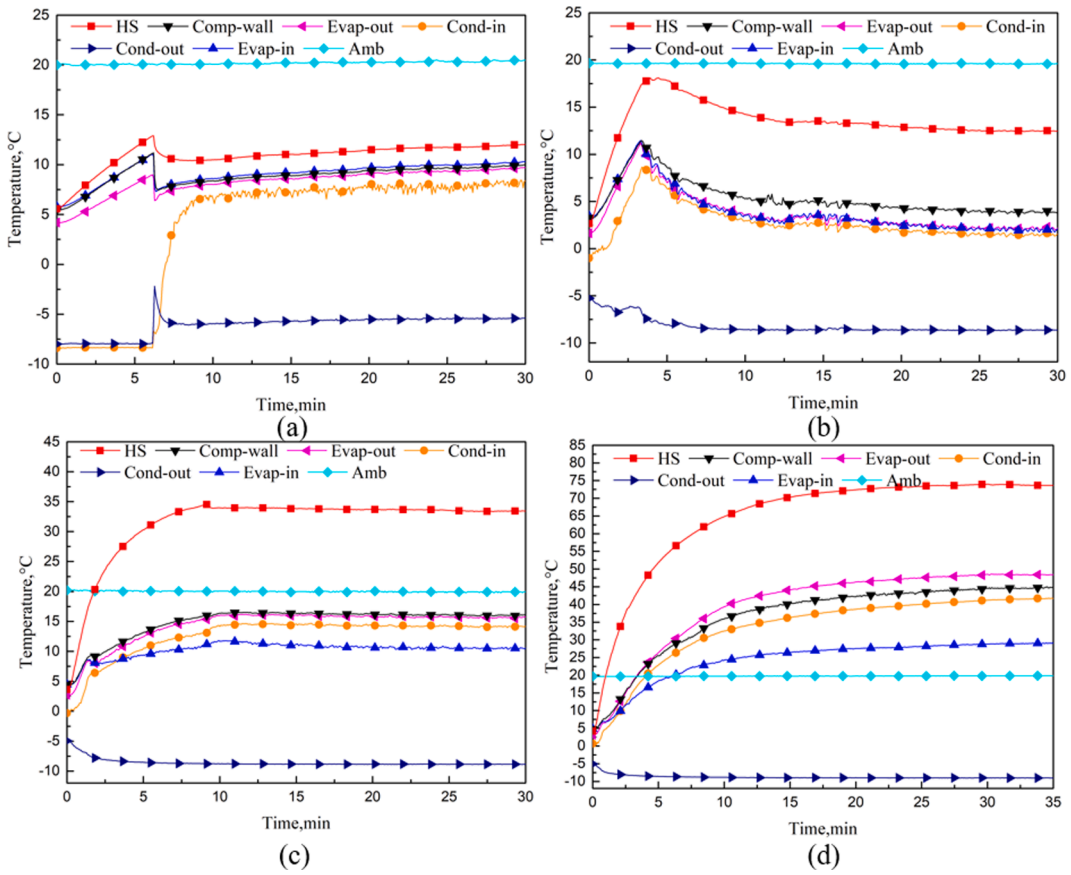

Fig. 6. The thermal performance in the start-up process with a heat sink temperature of −10 °C. (a) A heat load of 10 W. (b) A heat load of 50 W. (c) A heat load of 110 W. (d) A heat load of 190 W.

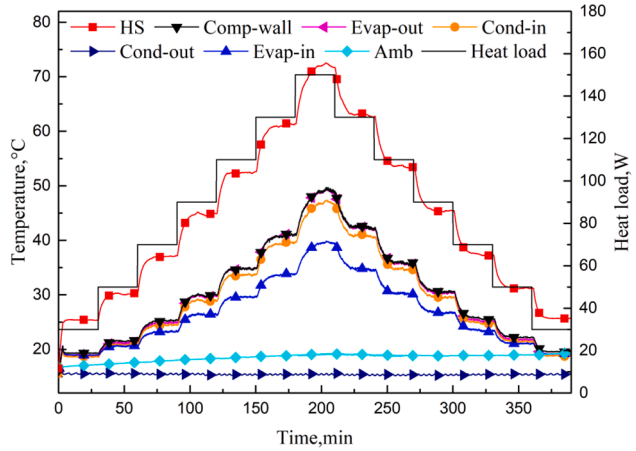

Fig. 7. The thermal performance under uniformly variable heat load with a heat sink temperature of 15 °C.

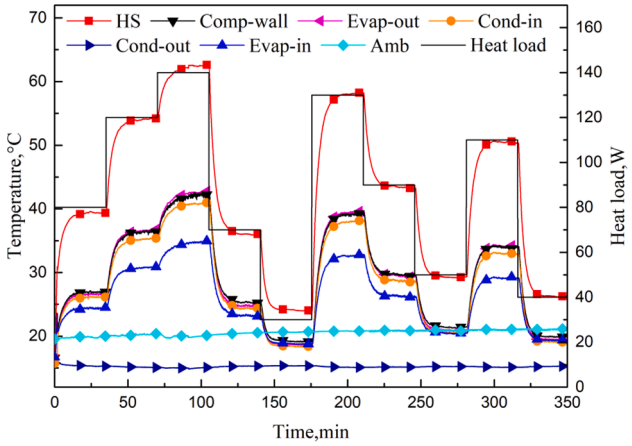

Fig. 8. The thermal performance under randomly variable heat load with a heat sink temperature of 15 °C.

sink temperature of −10 °C, 0 °C, and 15 °C, respectively.

According to the characteristic temperature curve, the LHP can be divided into two working modes, namely variable conductance mode and constant conductance mode. With a rise in the heat load, the temperature of the heating area remained stable or rose gently in the early stage. Under this condition, the growth in heat load resulted in not only an increase in the heat leakage from the heating area to the compensation chamber but also a rise in the amount of the subcooling of the liquid. Meanwhile, the impact of the environmental heat leakage was also reduced with a higher flow rate of the working fluid. The increment in subcooling degree could compensate for the increase in heat leakage from the heating area so that the evaporator temperature remained stable or grew slightly. However, as the heat load continued to rise, the condensing surface in the condenser was unable to continuously expand, so that the amount of supercooling carried by the return liquid had reached the upper limit. The heat leakage was not able to be mostly offset hence the temperature of the compensation chamber steeply rose and the working mode changed to the constant conductance mode from the variable conductance mode. The range of the variable conductance mode would be larger with a lower heat sink temperature because the

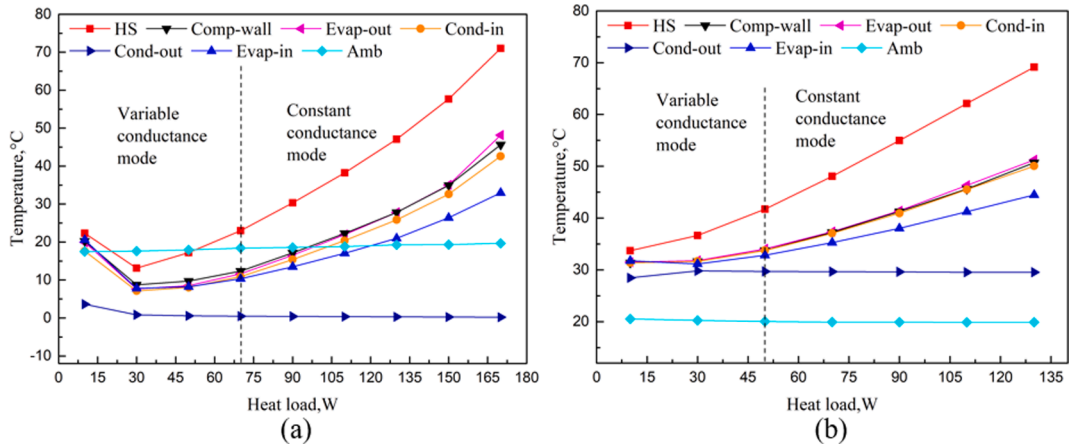

Fig. 9. The relationship between characteristic temperature and heat load. (a) the heat sink temperature of 0 °C. (b) the heat sink temperature of 30 °C.

leakage for the evaporator was compensated well. As illustrated in Fig. 9, the critical heat load was 70 W and 50 W with the heat sink temperature of 0 °C and 30 °C, respectively.

3.4. The thermal resistance analysis

According to the definition of thermal resistance, the thermal resistance of the evaporator and the total LHP can be calculated by the following Eq. (3) and Eq. (4),

$$R_{evap} = \frac{T_h - T_v}{Q} \tag{3}$$

$$R_{LHP} = \frac{T_h - T_c}{Q} \tag{4}$$

where T_h, T_v, and T_c denote the temperature of the heating area, the vapor outlet, and the condenser, respectively. T_c is the average value of the temperatures of the condenser inlet and outlet. Q denotes the applied heat load. Fig. 10 shows the relationship between the evaporator thermal resistance and the heat load at four heat sink temperatures. Contact thermal resistances, which should be controlled at a low level, are large parts of the evaporator thermal resistance. In order to get a low contact thermal resistance, several measures like using a higher pressure to compact the powder to ensure the flatness of the wick during its fabrication, adopting an interference fit between the wick and the evaporator shell to attain a close contact between the wick and the evaporator, applying high thermal conductive filled silicone paste between the heating module and the bottom of the evaporator, and using custom-made fixtures to clamp the evaporator and the heating surface, were obtained. Through the above measures, the evaporator thermal resistance had been maintained at a low level during the experimental tests.

During the operation, the capillary wick always remained saturated and the vaporization of the working fluid occurred only on the surface of the capillary wick, both of which resulted in a downward trend in the evaporator thermal resistance with growing heat load. Therefore, the minimum resistances were got at the maximum heat load under different heat sink temperatures, which were 0.137 °C/W (-10 °C), 0.134 °C/W (0 °C), 0.155 °C/W (15 °C), 0.138 °C/W (30 °C), respectively. Even with the maximum heat load, some potential points could be used as the cites of vaporization. Moreover, the vapor–liquid interface in the capillary wick could still extend. While the heat load continued to increase, the vapor would appear in the capillary wick, reducing the evaporator heat transfer capacity and bringing a turning point of the evaporator thermal resistance simultaneously.

As presented in Fig. 11, the total thermal resistances with four different heat sink temperatures had a similar relationship with the heat load. With the heat load increasing, the total thermal resistance bottomed out, then went up slightly. The minimum value (0.197 °C/W) was obtained when the heat load was 30 W with a heat sink temperature of 30 °C. The total thermal resistance was composed of two parts, namely the evaporator resistance and the condenser efficiency. There was an opposing tendency between the thermal resistance of the LHP and the evaporator in the post-middle stage, from which a drop in the

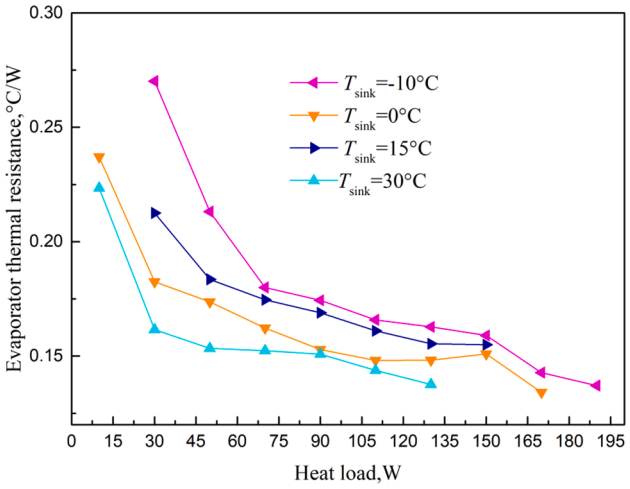

Fig. 10. The relationship between evaporator thermal resistance and heat load.

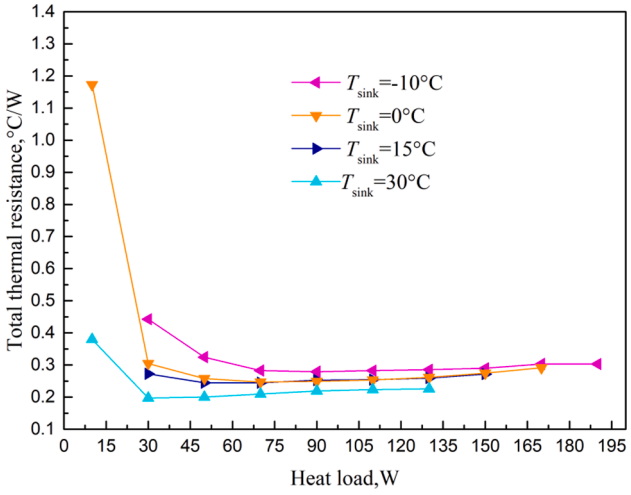

Fig. 11. The relationship between total thermal resistance and heat load.

condenser efficiency was deduced. Due to the lower latent heat of vaporization, the amount of the R1233zd(E) vaporization was larger than that of traditional fluids so the condensing surface had been fully utilized under a small heat load. After that, the increase in heat load would not cause an expansion of the condensing surface but a decline in the efficiency of the condenser. This was a disadvantage of R1233zd(E) while this condition can be improved by adding the length of the condenser or using other materials with better thermal conductivity.

Uncertainty is an index indicating the reliability of the measurement results, which can be calculated by

$$\frac{\Delta R_{LHP}}{R_{LHP}} = \sqrt{(\frac{\Delta s}{s})^2 + (\frac{\Delta Q}{Q})^2} \tag{5}$$

$$\Delta s = \sqrt{\sum_{i=1}^{4} (\frac{1}{4}\Delta T_{h,i})^2 + \sum_{j=1}^{2} (\frac{1}{2}\Delta T_{c,j})^2} \tag{6}$$

$$s = T_h - T_c \tag{7}$$

where $T_{h,i}$ is the temperature of the heating area measured by 4 thermocouples. $T_{c,j}$ is the temperature of the condenser inlet and outlet, respectively. The uncertainty of all T-type thermocouples used is 0.3 °C. As a consequence, the maximum uncertainty of the R_{LHP} was calculated to 6.51%. The minimum uncertainty was 0.67% with a heat load of 190 W.

4. Conclusions

In this paper, an eco-friendly flat-disk loop heat pipe with a nickel biporous capillary wick had been presented. The design of the aluminum alloy structure was for the consideration of weight and price, and environmental friendliness and non-toxicity to the human were the reasons for choosing R1233zd(E) as the working fluid. Experiments were carried out at four heat sink temperatures with the heating area temperature below 75 °C. Based on the experimental investigation and analysis, conclusions can be drawn as follows:

(1) The evaporator deformation did not occur and the LHP performed robust stability and reliability during long-time experimental tests. Aluminum alloy could reach the requirements in strength and it had good compatibility with nickel capillary wick and R1233zd(E).
(2) The temperature fluctuations were observed with low heat loads directly caused by intermittent replenishment of the compensation chamber. Under low heat loads, the vapor pressure dropped rapidly after the vapor entered the condenser, resulting in the inability to overcome the gravity head so the subcooled liquid could not return to the compensation chamber. With the increase in the heat load or the heat sink temperature, the temperature fluctuations disappeared.
(3) The LHP, with a 790 mm effective length, could dissipate the heat of 190 W (11.43 W/cm^2) with a heat sink temperature of −10 °C. Even the heat sink temperature was 30 °C, the maximum heat load could reach 130 W (7.82 W/cm^2) when the temperature of the heating area was 70.4 °C.
(4) The minimum thermal resistance of the evaporator was 0.134 °C/W when the heat load was 170 W with a 0 °C heat sink temperature. The minimum thermal resistance of the total LHP was 0.197 °C/W when the heat load was 30 W with a 30 °C heat sink temperature.

Declaration of Competing Interest

The authors declare that they have no known competing financial interests or personal relationships that could have appeared to influence the work reported in this paper.

Acknowledgment

The work was supported by the National Natural Science Foundation of China (Grant No. 51736004 and No. 51776079).

References

[1] Y.F. Maydanik, Loop heat pipes, Appl. Therm. Eng. 25 (2005) 635–657.
[2] Y.F. Maydanik, M.A. Chernysheva, V.G. Pastukhov, Review: loop heat pipes with flat evaporators, Appl. Therm. Eng. 67 (2014) 294–307.
[3] C. Nadjahi, H. Louahlia, S. Lemasson, A review of thermal management and innovative cooling strategies for data center, Sustain. Comput. Inf. Syst. 19 (2018) 14–28.
[4] J. Choi, M. Jeong, Preliminary design on high-end workstation cooling system using loop heat pipes, Therm. Sci. Eng. Progr. 20 (2020) 100519, https://doi.org/10.1016/j.tsep.2020.100519.
[5] S. Du, Q. Zhang, P. Hou, C. Yue, S. Zou, Experimental study and steady-state model of a novel plate loop heat pipe without compensation chamber for CPU cooling, Sustain. Cities Soc. 53 (2020) 101894, https://doi.org/10.1016/j.scs.2019.101894.
[6] G. Zhou, J. Li, Z. Jia, Power-saving exploration for high-end ultra-slim laptop computers with miniature loop heat pipe cooling module, Appl. Energy 239 (2019) 859–875.
[7] Z. Zhang, H. Zhang, Z. Ma, Z. Liu, W. Liu, Experimental study of heat transfer capacity for loop heat pipe with flat disk evaporator, Appl. Therm. Eng. 173 (2020) 115183, https://doi.org/10.1016/j.applthermaleng.2020.115183.
[8] A.B. Solomon, A.K. Mahto, R.C. Joy, A.A. Rajan, D.A. Jayprakash, A. Dixit, A. Sahay, Application of bio-wick in compact loop heat pipe, Appl. Therm. Eng. 169 (2020) 114927, https://doi.org/10.1016/j.applthermaleng.2020.114927.
[9] J. Liu, Y. Zhang, C. Feng, L. Liu, T. Luan, Study of copper chemical-plating modified polyacrylonitrile-based carbon fiber wick applied to compact loop heat pipe, Exp. Therm Fluid Sci. 100 (2019) 104–113.
[10] Z. Zhang, R. Zhao, Z. Liu, W. Liu, Application of biporous wick in flat-plate loop heat pipe with long heat transfer distance, Appl. Therm. Eng. 184 (2021) 116283, https://doi.org/10.1016/j.applthermaleng.2020.116283.
[11] N. Phan, H. Nagano, Fabrication and testing of a miniature flat evaporator loop heat pipe with polydimethylsiloxane and molding, Appl. Therm. Eng. 175 (2020) 115377, https://doi.org/10.1016/j.applthermaleng.2020.115377.
[12] J. Xu, D. Wang, Z. Hu, L.i. Zhang, L.i. Ye, Y. Zhou, Effect of the working fluid transportation in the copper composite wick on the evaporation efficiency of a flat loop heat pipe, Appl. Therm. Eng. 178 (2020) 115515, https://doi.org/10.1016/j.applthermaleng.2020.115515.
[13] M.A. Chernysheva, S.I. Yushakova, Y.F. Maydanik, Effect of external factors on the operating characteristics of a copper–water loop heat pipe, Int. J. Heat Mass Transf. 81 (2015) 297–304.
[14] K. Odagiri, H. Nagano, Heat transfer characteristics of flat evaporator loop heat pipe under high heat flux condition with different orientations, Appl. Therm. Eng. 153 (2019) 828–836.
[15] A.R. Anand, A. Jaiswal, A. Ambirajan, P. Dutta, Experimental studies on a miniature loop heat pipe with flat evaporator with various working fluids, Appl. Therm. Eng. 144 (2018) 495–503.
[16] H. Wang, G. Lin, X. Shen, L. Bai, R. Yang, D. Wen, Effect of evaporator/condenser elevations on a loop heat pipe with non-condensable gas, Appl. Therm. Eng. 180 (2020) 115711, https://doi.org/10.1016/j.applthermaleng.2020.115711.
[17] J. Li, L. Lv, Performance investigation of a compact loop heat pipe with parallel condensers, Exp. Therm Fluid Sci. 62 (2015) 40–51.
[18] S. He, J. Zhao, Z.-C. Liu, W. Tian, J.-G. Yang, W. Liu, Experimental investigation of loop heat pipe with a large squared evaporator for cooling electronics, Appl. Therm. Eng. 144 (2018) 383–391.
[19] Y. Aono, N. Watanabe, A.i. Ueno, H. Nagano, Development of a loop heat pipe with kW-class heat transport capability, Appl. Therm. Eng. 183 (2021) 116169, https://doi.org/10.1016/j.applthermaleng.2020.116169.
[20] B. Xiao, W. Deng, Z. Ma, S. He, L. He, X. Li, F. Yuan, W. Liu, Z. Liu, Experimental investigation of loop heat pipe with a large squared evaporator for multi-heat sources cooling, Renew. Energy 147 (2020) 239–248.
[21] A. Ueno, S. Tomita, H. Nagano, Experimental investigation on a thin-loop heat pipe with new evaporator structure, J. Heat Transfer 143 (2021).
[22] T. Shioga, Y. Mizuno, H. Nagano, Operating characteristics of a new ultra-thin loop heat pipe, Int. J. Heat Mass Transf. 151 (2020) 119436, https://doi.org/10.1016/j.ijheatmasstransfer.2020.119436.
[23] G. Zhou, J. Li, L. Lv, An ultra-thin miniature loop heat pipe cooler for mobile electronics, Appl. Therm. Eng. 109 (2016) 514–523.
[24] J. Xu, L. Zhang, H. Xu, J. Zhong, J. Xuan, Experimental investigation and visual observation of loop heat pipes with two-layer composite wicks, Int. J. Heat Mass Transf. 72 (2014) 378–387.
[25] Z. Liu, H. Li, B. Chen, J. Yang, W. Liu, Operational characteristics of flat type loop heat pipe with biporous wick, Int. J. Therm. Sci. 58 (2012) 180–185.
[26] S. He, Z. Liu, D. Wang, J. Zhao, W. Liu, J. Yang, Investigation of the flat disk-shaped LHP with a shared compensation chamber, Appl. Therm. Eng. 104 (2016) 139–145.

[27] Y. Maydanik, M. Chernysheva, S. Vershinin, High-capacity loop heat pipe with flat evaporator for efficient cooling systems, J. Thermophys Heat Transfer 34 (2020) 465–475.
[28] Z. Wan, J. Deng, B. Li, Y. Xu, X. Wang, Y. Tang, Thermal performance of a miniature loop heat pipe using water–copper nanofluid, Appl. Therm. Eng. 78 (2015) 712–719.
[29] J.i. Li, G. Zhou, T. Tian, X. Li, A new cooling strategy for edge computing servers using compact looped heat pipe, Appl. Therm. Eng. 187 (2021) 116599, https://doi.org/10.1016/j.applthermaleng.2021.116599.
[30] Y. Maydanik, V. Pastukhov, M. Chernysheva, Development and investigation of a loop heat pipe with a high heat-transfer capacity, Appl. Therm. Eng. 130 (2018) 1052–1061.
[31] G.A. Longo, S. Mancin, G. Righetti, C. Zilio, J. Steven Brown, Brown, Assessment of the low-GWP refrigerants R600a, R1234ze(Z) and R1233zd(E) for heat pump and organic Rankine cycle applications, Appl. Therm. Eng. 167 (2020) 114804, https://doi.org/10.1016/j.applthermaleng.2019.114804.
[32] M.O. McLinden, A.F. Kazakov, J. Steven Brown, P.A. Domanski, A thermodynamic analysis of refrigerants: possibilities and tradeoffs for Low-GWP refrigerants, Int. J. Refrig 38 (2014) 80–92.
[33] B.J. Huang, H.H. Huang, T.L. Liang, System dynamics model and startup behavior of loop heat pipe, Appl. Therm. Eng. 29 (2009) 2999–3005.